Nanoparticles Encapsulated in Porous Carbon Matrix Coated on Carbon Fibers: An Ultrastable Cathode for Li-Ion Batteries

Rujia Zou, Qian Liu, Guanjie He, Muk Fung Yuen, Kaibing Xu, Junqing Hu,* Ivan P. Parkin, Chun-Sing Lee,* and Wenjun Zhang*

Dr. R. Zou, Dr. Y. Liu, Dr. K. Xu, Prof. J. Hu

State Key Laboratory for Modification of Chemical Fibers and Polymer Materials, College of Materials Science and Engineering, Donghua University, Shanghai 201620, China

E-mail: hu.junqing@dhu.edu.cn

Dr. M. Yuen, Prof. C. Lee, Prof. W. Zhang

Center of Super-Diamond and Advanced Films (COSDAF), Department of Physics and Materials Science, City University of Hong Kong, Hong Kong

E-mail: apcslee@cityu.edu.hk; and apwjzh@cityu.edu.hk

Dr. G. He, Prof. I. Parkin

Materials Chemistry Centre, Department of Chemistry, University College London, 20 Gordon Street, London WC1H 0AJ, UK

Abstract text.

Nanostructured V_2O_5 is emerging as a new cathode material for lithium ion batteries for its distinctly high theoretic capacity over the current commercial cathodes.

The main challenges associated with nanostructured V_2O_5 cathodes are structural degradation, instability of the solid-electrolyte interface (SEI) layer and poor electron conductance, which lead to low capacity and rapid decay of cyclic stability. Here, we report a novel composite structure of V_2O_5 nanoparticles encapsulated in 3D networked porous carbon matrix coated on carbon fibers (V_2O_5/3DC-CFs) that effectively address the mentioned problems. Remarkably, the V_2O_5/3DC-CFs electrode exhibits excellent overall lithium-storage performance, including high Coulombic efficiency, excellent specific capacity, outstanding cycling stability and rate property. A reversible capacity of ~ 183 mAh g^{-1} was obtained at the high current density of 10 C, and the battery retained 185 mAh g^{-1} after 5000 cycles, which to our knowledge shows the best cycling stability reported to date among all reported cathodes of lithium ion batteries. The outstanding overall properties of the V_2O_5/3DC-CF composite make it a promising cathode material of lithium ion batteries for the power-intensive energy storage applications.

1. Introduction

The increasing demands for lithium-ion batteries (LIBs) for power-intensive energy storage applications such as electric vehicles and load-leveling installations on power grids require improved energy and power densities as well as better durability.[1-3] In the LIB techniques, the development of new electrode materials has been identified to be a key for their further advances. Various anode materials have been substantially studied and made great progress in recent years.[4,5] For instance, Si-based nanostructures showed much improved capacity and superior cyclability, e.g., a high specific capacity of ~1200 mAh·g^{-1} (3 times greater than that of graphite, 372 mAh·g^{-1}) with a capacity retention of 97% after 1000 cycles has been achieved.[6] In contrast, research on the cathode materials of high specific capacity is severely lagging behind

that of the anode materials, and it has been regarded a bottleneck for the power-intensive energy storage applications of LIBs. In order to promote the development of high-performance LIBs, the new LIB cathode structures and materials have attracted broad research interest recently.[7-10] For instance, the $Li_4Mn_2O_5$ composition electrode delivered a high discharge capacity of 355 mAh g^{-1} between 1.2 and 4.8 V at a current density of 0.05 C, however, the capacity retention was about 70.4 % after 9 cycles.[8] The $LiNi_{0.4}Mn_{0.4}Co_{0.2}O_2$ cathode materials showed a discharge capacity of 228 mAh g^{-1} at the first cycle, and its capacity retention was ~ 96 % after 20 cycles between 2.0 and 4.7 V at a current density of 0.05 C.[9] The $Li_2Ru_{0.75}Ti_{0.25}O_3$ presented a capacity of 215 mAh g^{-1} between 2.7 and 4.5V at 0.2C, with a capacity retention of ~90 % after 100 cycles.[10] It appears that the most important challenge ahead is to improve the cycling stability of cathode at high rating, and this is a major gap in the development of high-performance LIBs.

Recently, vanadium oxides have drawn great research interest due to their intriguing advantages as a cathode material.[11,12] For instance, V_2O_5 can capture multiple electrons and have a high capacity of 294 mA h g^{-1} in the voltage range of 4.0-2.0 V (vs Li/Li$^+$), which are higher than those of commercial cathode materials (e.g., 140 mA h g^{-1} for $LiCoO_2$, 148 mA h g^{-1} for $LiMn_2O_4$, and 170 mA h g^{-1} for $LiFePO_4$).[6,13-15] In addition, V_2O_5 is abundant in the earth's crust and of low cost. Nevertheless, the low Li$^+$ diffusion coefficient (~10^{-12} cm^2 s^{-1}) in V_2O_5 and the moderate electron conductance between V_2O_5 and binders lead to poor cycling stability and low capacity.[16,17] To solve these problems, various approaches have been suggested, e.g., engineering of nanoscaled architectures with reduced ion/electron transportation paths,[18-23] growth of three-dimensional (3D) structures on carbon nanotubes,[24,25] and coating of conductive layers on active materials for improving electrical contact.[26-28] Preparation of a V_2O_5-based electrode

typically involves pressing a mixture of V_2O_5 powder, carbon black and polymer binders onto a current collector. There is considerable interparticle resistance in the composite which hinders charge transfer and reduces battery performance.[17,29] **Recently, it was shown that direct growth of V_2O_5 array structures on a current collector can substantially reduce the interparticle resistance and contact resistance, and leads to improved capacity and cyclic stability**.[30-32] However, the low areal loading of the V_2O_5 array structures ($\sim$0.7 mg cm^{-2}), hindered their practical application.[33] Moreover, collapse of the V_2O_5 array structures upon repeated charge/discharge cycling is another important problem to be addressed for high-performance LIBs.[34]

Here, we present a LIB cathode comprising V_2O_5 nanoparticles encapsulated in a 3D networked porous carbon matrix on carbon fibers (V_2O_5/3DC-CFs) for the first time. The 3D networked porous carbon not only enables effective mass loading of V_2O_5 nanoparticles and providing extensive reaction sites but also acts as an electrolyte-blocking layer to reduce SEI formation on surface of the V_2O_5 nanoparticles. Moreover, the direct use of 3DC-CFs as a current collector eliminates the need of using conductive additives and binders, and guarantees a good electrical conductance. The special material composition and structure design endow the cathode with a much improved irreversible capacity of $\sim$ 183 mAh g^{-1} at a high current density of 10 C over the voltage range of 4.0-2.0 V. Particular, the capacity retained at 185 mAh g^{-1} after 5000 charge/discharge cycles, which is to our knowledge the best cycling stability among all reported cathodes in half-cell of LIBs. These results suggest that the V_2O_5/3DC-CFs is a promising material for cathode application in high-performance LIBs and flexible LIBs.

2. Results and Discussions

The 3DC layer was prepared by carbonization of a polymer film formed by a sol-gel process, and the V_2O_5 nanoparticles encapsulated in the carbon matrix were synthesized using a hydrothermal reaction followed by a post annealing process. Detailed synthesis conditions are described in Supplementary Information. **Figure 1**a shows a low-magnification SEM image of a bundle of flexible CFs coated with a layer of carbon precursor. Upon carbonization, the layer was converted to uniformly 3D porous carbon film covering the entire surface of each CF (Figures 1b-d). The diameter of the CFs increased slightly from ~8 · m to ~10 · m upon carbonization (Figure 1b). **Raman spectrum in Figure S1 shows D peak at ~1340 cm^{-1} and G peak at ~1590 cm^{-1}, suggesting that the porous layer consists of both disordered and graphitic carbon structures.** Close observation (Figures 1c and 1d) reveals that the carbon layer composes of interconnected and intersected carbon nanoflakes, giving a 3D networked structure similar to that of a sponge. The carbon nanoflakes had a thickness < 100 nm (Figure 1d). A TEM image (Figure S2) also confirmed that the carbon nanoflakes were interconnected with each other to form a 3D networked matrix containing irregularly pores with the size ranging from 30 to 80 nm. **N$_2$ isotherm adsorption/desorption measurements were carried out to characterize the networked porous carbon matrix, as shown in Figure S3. The porous matrix exhibited a Brunauer-Emmett-Teller (BET) specific surface area of 493 m^{2}g^{-1}.**

After hydrothermal reaction followed by a post annealing process, V_2O_5 nanoparticles were synthesized inside the pores in the 3DC-CFs to form a V_2O_5/3DC-CFs composite. The composite retains well the original morphology of the 3DC-CFs, as shown in Figure 1e. The V_2O_5/3DC-CFs composite presents excellent flexibility (Figure S4), making it a highly promising candidate as flexible electrodes for LIB application in

wearable electronics. Figure 1f (upper panel) depicts an XRD pattern of the V_2O_5/3DC-CFs composite. The broad diffraction peak at $\sim 27º$ is indexed to the (002) plane of graphitic carbon (CFs and carbon nanoflakes). With reference to an XRD pattern for the orthorhombic V_2O_5 (lower panel of Figure 1f), it can be confirmed that phase-pure orthorhombic V_2O_5 was obtained. Energy dispersive X-ray spectroscopy (EDS) elemental mapping images of a V_2O_5/3DC composite in Figure S5 suggest that the V_2O_5 nanoparticles have a uniform distribution in the 3DC matrix layer. The amount of V_2O_5 nanoparticle loading could be controlled by changing the thickness of 3DC layer on CFs.

Figure 1g shows a TEM image of the V_2O_5 nanoparticles grown on a carbon nanoflake. It can be seen that V_2O_5 nanoparticles are anchored on the surface of carbon nanoflakes. Thus in the 3D networked matrix they are encapsulated in the pores formed by carbon flakes. The size of V_2O_5 nanoparticles varies from 20 to 30 nm, as shown in Figure 1g. An HRTEM image of a V_2O_5 nanoparticle in Figure 1h reveals the crystalline nature of the V_2O_5 nanoparticles, and the observed d-spacing of 0.44 nm matches well with that of the {001} facets of orthorhombic V_2O_5. The corresponding Fast Fourier Transform (FFT) pattern in the inset agrees with that obtained along the [100] zone axis of orthorhombic V_2O_5.

Figure 1

Electrochemical performance of the V_2O_5/3DC-CFs composite with a V_2O_5 nanoparticle (active material) areal loading density of 1.18 mg cm^{-2} was evaluated. **Figure 2**a displays **representative CV curves for the 1st, 2nd and 5th cycles at a scan rate of 0.1 mVs^{-1} over a voltage window of 4.0-2.0 V *vs* Li/Li$^+$**. In the first cycle, the

reduction peak at 3.4 V corresponds to a phase change from α-V_2O_5 to ϵ-$Li_{0.5}V_2O_5$; and peaks at 3.1 V and 2.3 V are assigned to the formation of δ-LiV_2O_5 and γ-$Li_2V_2O_5$, respectively.[19-22] In the delithiation process, three anodic peaks at 2.5, 3.3 and 3.5 V are revealed, and they are ascribed to the corresponding reversed phase transformations from γ-$Li_2V_2O_5$ to δ-LiV_2O_5, ϵ-$Li_{0.5}V_2O_5$, and α-V_2O_5, respectively[35]. The CV curves for the 2nd and 5th cycles resembled that of the 1st cycle suggesting an excellent reversibility of the cycling process.

Figure 2b shows representative charge-discharge curves of the electrode at a current density of 0.1C (1C=294 mA h g^{-1}) for the first three cycles. Three plateaus at 3.4, 3.1 and 2.3 V were observed on the discharge curves, which are associated with the multi-step Li^+ intercalation processes. Correspondingly, three plateaus related to the delithiation processes were also detected at 2.5, 3.3 and 3.5 V on the charge curves. The charge-discharge curves are in good agreement with the CV results. The first cycle revealed a high capacity of 360.6 mAh g^{-1}. The irreversible capacity loss for the first cycle can be attributed to the formation of a solid-electrolyte interface (SEI) layer. In the second and third cycles, the capacities of the electrode decreased to 339.8 mAh g^{-1} and 339.2 mAh g^{-1}, respectively, and the corresponding Coulombic efficiency increased to 99.8% and 99.9%, respectively. The sharp increase of Coulombic efficiency in the 2nd cycle indicates that a stable SEI layer had already formed during the initial cycle. **It is noted that the measured capacity of the electrode (339.8 mAh g^{-1}) is higher than the theoretic capacity of V_2O_5 (294 mAh g^{-1}), which is considered to be due to the following reasons: Firstly, the V_2O_5 nanoparticles have a large surface-to-volume ratio and the short transport length of Li^+ ions, which may provide more active sites for the redox reactions of Li^+ ions as compare with the bulk V_2O_5. The similar results have been observed in other nanostructured metal oxide including**

V_2O_5.[36-38] Secondly, the uncertainty in the average mass of V_2O_5 (about ± 5%) may also lead to an error of about ± 5% in the calculation of corresponding specific capacity. It should be noted that, for a cathode electrode material of LIBs, a higher discharge voltage plateau is favorable for releasing more energy. In the case of the V_2O_5/3DC-CFs composite, the capacity delivered in the high-voltage range from 4.0 to 3.0 V (denoted by horizontal green dashed line) accounts for more than 62.4% of the total capacity between 4.0 and 2.0 V (vs Li/Li^+). The capacity was estimated to be $\sim$212.1 mAh g^{-1} (the second cycle) at a current density of 0.1C in the high-voltage range from 4.0 to 3.0 V, which is still higher than those of the commonly used cathode materials such as $LiCoO_2$ (140 mA h g^{-1}), $LiMn_2O_4$ (148 mA h g^{-1}) and $LiFePO_4$ (170 mA h g^{-1}).[14-16] The capacity of the V_2O_5/3DC-CFs composite electrode in this voltage region is also apparently higher than those of the V_2O_5 nanostructure electrodes reported in the literature.[21-27] The cathode material of high-voltage plateau is necessary for increasing the operating voltage of lithium-ion batteries and, subsequently, enhancing the energy density. To have a fair comparison with the results reported previously, the capacities reported below in this work are, however, the total capacities measured for the voltage range from 4.0 to 2.0 V.

The rate capability (0.1-50 C) of the V_2O_5/3DC-CFs composite electrode was evaluated in the voltage range of 4.0-2.0 V, as presented in Figure 2c. The capacities decreased from $\sim$330 to 285, 220, 176, 138, and 115 mAh g^{-1} when the current density was increased from 0.1 to 1, 5, 10, 30, and 50 C, respectively. Note that a capacity of 115 mAh g^{-1} was retained at a high current density of 50 C. After cycling at a current density of 50 C, the capacity could be recovered to about 310 mAh g^{-1} as the current density was decreased back to 0.1 C, which corresponds to capacity retention of $\sim$ 94% and indicates an excellent reversibility of the electrode.

A major concern for the application of V_2O_5 as a cathode material is on its unsatisfactory cycling stability. In this work, the cycling stability of the V_2O_5/3DC-CFs cathode was tested by carrying out the discharge-charge cycles at a current density of 1C, as shown in Figure 2d (blue and black denotes for the discharge and charge curves, respectively). The discharge capacity was 283 mAh g^{-1} in the second cycle (the first cycle for the activation of V_2O_5), and the capacity maintained at 281 mAh g^{-1} after 120 cycles, corresponding to a capacity retention of 99.3%. On average, V_2O_5/3DC-CFs composite electrode showed a capacity fading rate of only 0.0059% per cycle, which is least two orders of magnitude smaller than those of previously reported V_2O_5-based cathodes.[19-29] In addition, a high Coulombic efficiency close to 100% (except for the first few cycles) was achieved, and it was very stable in the following 120 cycles (red curve), suggesting an excellent reversibility of the electrode. It should be pointed out that the corresponding evaluation on the capacity and stability of sole carbon cloth (Figure S6) verified that 3DC-CFs had only negligible contribution to the overall capacity of V_2O_5/3DC-CFs composite electrodes (~6 mAh g^{-1} out of 1 C).

Remarkably, the V_2O_5/3DC-CFs composite electrodes still exhibited extremely good stability at a high current density of 10 C (Figure 2e). The capacity was 183 mAh g^{-1} in the second cycle at 10 C, and it kept almost unchanged after 5000 cycles (red and black curves for the discharge and charge processes, respectively), which represents the best stability among all nanostructured materials reported thus far for LIB application,[39-41] including V_2O_5 nanostructures.[19-29] In addition, except for the first few cycles, the Coulombic efficiency of the V_2O_5/3DC-CFs composite electrode was stabilized at ~100% (orange curve in Figure 2e). For comparison, the control samples, pure V_2O_5 nanoparticles (left inset in Figure 2e and Figures S7a and b) and V_2O_5 nanosheet arrays on CFs (right inset in Figure 3e and Figures S7c and d) were synthesized and their cyclic

stabilities as cathodes were also tested at 10 C, as shown in Figure 2e. The V_2O_5 nanoparticle electrode was prepared in a conventional way by mixing the V_2O_5 nanoparticles with binder and conductive carbon. In sharp contrast to the V_2O_5/3DC-CFs composite, the capacities of the V_2O_5 nanoparticles (blue and pink curves for the discharge and charge curves) and V_2O_5 nanosheet arrays (green and light blue curves for the discharge and charge curves) electrodes declined drastically from ~142 mAh g^{-1} and ~155 mAh g^{-1} in the second cycle to 9 mAh g^{-1} and ~15 mAh g^{-1} after 5000 cycles, respectively.

Effective areal loading of active materials in the electrode is another important issue in LIBs for their practical applications, and a high loading amount will generally lead to decreased capacity and stability. In this work the impacts of mass loading of V_2O_5 on the capacity and stability were also studied, and the amount of active material loading was controlled by varying the thickness of carbon matrix films on CFs. **From cross-sectional morphology of the 3D carbon layer occasionally observed on the sample synthesized by soaking carbon cloth for four times in the sol-gel solution followed by carbonization, the thickness of 3D carbon layer is about 1.9 μm, as shown inset Figure 2f. Therefore each cycle of soaking and carbonization may result in a thickness of about 0.5 μm of 3D carbon layer.** For the active materials of 0.52, 2.48 and 3.17 mg cm^{-2} in diferent samples, capacities of 175, 175, and 186 mAh g^{-1} were obtained, respectively, in the second cycle at 10C, and they maintained unchanged after 1000 cycles (Figure 2f). The uncertainty in the average mass of 3DC-CFs thus led to an error of about ± 5% in the mass of V_2O_5 and the calculation of corresponding specific capacity. Considering the error, the specific capacities obtained for the different mass loadings could be considered almost unchanged. The capacity retention was close to 100% after 1000 cycles for all samples, suggesting an excellent cycling stability of the

V_2O_5/3DC-CFs composite electrodes even with relatively high loadings of active materials. Moreover, it was also observed that electrochemical performance of electrodes depends also on the size of V_2O_5 nanoparticles. For the V_2O_5 nanoparticles with mean size of ~40 to ~50 nm (Figure S8), the corresponding capacities were 161 and 172 mAh g^{-1}, respectively, in the second cycle at 10 C, and they decreased to 153 and 151 mAh g^{-1} after 1000 cycles, suggesting capacity retentions of 95% and 88% respectively. Whereas, with a particle size of ~20 nm, the capacity remained close to 100% after 1000 cycles (Figure 2f). The better performance for the smaller particle size, may be ascribed to the increased surface area, the shorter ion diffusion length, and better capability in maintaining structural integrity for electrochemical reactions.[42,43]

Figure 2

Generally, the formation of a thick and/or unstable SEI layer caused by repeated formation of fresh SEI layer upon cycles of expansion/contraction of the electrode is one major cause for capacity fading in LIBs. To understand the outstanding electrochemical performance of the V_2O_5/3DC composite, we investigated its structural evolution upon Li$^+$ insertion and extraction processes via *in situ* TEM experiments. The set-up for the *in situ* TEM measurements is shown schematically in **Figure 3**a.[44] A piece of V_2O_5/3DC composite was attached to a Cu wire probe, and a small piece of Li/electrolyte was attached to the tip of an opposite W wire probe. By manipulating a piezoelectric motor on the TEM holder, the V_2O_5/3DC composite was moved to contact the Li/electrolyte, and a bias voltage of -4.0 V was then applied to drive Li ions to go through the electrolyte towards V_2O_5/3DC composite. Figure 3b depicts the pristine V_2O_5/3DC composite before upon Li$^+$ insertion processes. For the V_2O_5 nanoparticle at the edge of

the composite (marked by the blue circle), discernible structural changes of V_2O_5 nanoparticles can be observed during Li^+ insertion processes for 1 min to 20 min (Figures 3c-e). **A thin SEI layer could be observed after discharging for only 1 min (Figure 3c),[45] and the thickness of SEI layer increased gradually during Li^+ insertion processes and reached about 5 nm after 20 mins (Figure 3e).** After 20 minutes of Li^+ deposition, no further structural change could be observed, indicating completion of the reaction (Figure S9). The V_2O_5 nanoparticle shows a dimension increase of ~20%, while no cracking or fracture was observed. In a sharp contrast, no obvious SEI layer could be observed on the V_2O_5 particles within the 3DC structures (marked by the red circle), as demonstrated in Figures 3f-h.

After the Li^+ insertion processed for 20 min, the delithiation was initiated by applying a 4.0 V bias to the V_2O_5/3DC composite electrode. The V_2O_5 nanoparticles slightly shrank in size, and the whole structure of V_2O_5/3DC composite remained unchanged after the delithiation finished, as shown in Figure 3i. Interesting, even after 10 lithiation and delithiation cycles (Figure 3j), the V_2O_5 nanoparticle inside the matrix had still no obvious SEI layer formed on its surface (red circle), possibly due to that the electrolyte only contacted with the outer surface of the robust ensemble of 3DC-CFs and did not access to the inner pores of the 3DC structure. These observations suggest that the engineered 3DC structure can provide an electrolyte blocking layer to decrease significantly most of the direct SEI formation on the V_2O_5 nanoparticles inside 3DC structure, and thus lead to superior cycling performance of the composite.

Figure 3

Morphologies of the V_2O_5/3DC-CFs composite electrode after 5000 cycles at 10 C were also examined with SEM and TEM (Figure S10). It was found that the V_2O_5/3DC architecture was well preserved without any apparent destruction. SEI layer was not also observed on the surface of the V_2O_5 particles inside the 3DC structure after 5000 cycles. In comparison, particulate aggregate (Figures S11a and b) and array structures collapse (Figures S11c and d) were revealed for the control samples of V_2O_5 nanoparticles and V_2O_5 nanosheet arrays after 5000 cycles, which is believed to the reasons for their inferior cycling stability.

Moreover, electrochemical impedance spectra (EIS) of the electrodes made of the V_2O_5/3DC-CFs composite, the V_2O_5 nanoparticles and the V_2O_5 nanosheet arrays after different cycles were shown in **Figure** 4a, Figure S12, and Table S1. The Nyquist plots of all samples depict a semicircle at high-to-medium frequency region and an inclined line at low frequency region.[46] The semicircle is attributed to the charge transfer process at electrode/electrolyte interface, while the inclined line corresponds to the lithium-diffusion process into the bulk of the electrode, the so-called Warburg diffusion. Figure 4b is a modified equivalent circuit model of the studied system.[47,48] For the V_2O_5/3DC-CF composite electrode, the fitted impedance parameter R_{ct} deceased gradually from ~121 to 88 Ω as the test extended from 100th to 5000th cycles, as shown in Figure 4a. Meanwhile, R_{ct} shows only mild change. As references, R_{ct} of the V_2O_5 nanoparticle electrode (Figure S12a) increased obviously from 1.4 to 4.5 kΩ, and similarly, R_{ct} of the V_2O_5 nanosheet array electrode increased from 71 to 168 Ω during the cycling process from 100th to 5000th cycle (Figure S12b), which should be associated with the deterioration of electron transport due to the formation of disconnected clusters by aggregation of nanoparticles and gradual array collapse during cycling.[32,46,49] Moreover,

R_s of the V_2O_5 nanosheet array electrode increased from 6.4 to 22.5 Ω from 100th to 5000th cycle, which could be caused by the dissolution of active materials into electrolyte during cycling processes. In comparison with the V_2O_5 nanoparticle and the V_2O_5 nanosheet array electrodes, the V_2O_5/3DC-CFs composite shows the smallest change in R_{ct} during long cycling. As a result, the V_2O_5/3DC-CFs composite provided significant advantages of rapid electron transport and fast faradic reaction during the electrochemical lithium insertion/extraction processes, which are favorable for increased capacity and longer cycling life.

Based on the above analysis, the following four strategically interdependent characteristics of the V_2O_5/3DC-CFs composite are responsible for its outstanding cathode performance, as illustrated schematically in Figure 4c. Firstly, the robust 3D interconnected carbon matrix with high conductivity provides highly efficient pathways for the fast electron/ion transfer in the electrodes (Figure 4d) and retains the structural integrity of the V_2O_5/3DC-CFs during charging/discharging processes. The pore structure of carbon framework also provides sufficient free space for the expansion of encapsulated V_2O_5 nanoparticles (Figure S13). After 5000 cycles, no obvious morphology change of the V_2O_5/3DC-CFs composite can be observed (Figure S10), which guarantees its excellent super-long cycling stability. Secondly, the electrode of the V_2O_5/3DC-CFs is fundamentally different from previously reported electrodes. In this design, the electrolyte only contacts with the carbon framework and cannot access the inner V_2O_5 particles, which prevents the inner V_2O_5 particles from reacting with electrolyte, i.e., the 3DC-CFs structure provides an electrolyte-blocking layer that limits the formation of SEI layer on the surface of most of the V_2O_5 nanoparticles (Figure 4d). As a result, the V_2O_5/3DC structure limits the amount of SEI layer and better utilization of active materials and electrolyte, which increases the Coulombic efficiency and

improves cycle stability. Thirdly, each V_2O_5 nanoparticle is directly anchored on the carbon nanoflakes of the 3D networked matrix, and the composite is used directly used as a cathode without the addition of binders. This not only ensure a more direct electrical path, but also **eliminate** the need for non-active binder material for weight and cost saving. Therefore, the resistance of the cathode is minimized, and Li^+ and electron transport to V_2O_5 nanoparticles is facilitated (Figure 4d). Finally, the optimized size of V_2O_5 nanoparticles reduces the solid state Li^+/electron diffusion length, prevents fracture, and increases active sites. Consequently, the ultrafast lithium storage in V_2O_5 can be realized, which guarantees a large capacity and super-long stability at high current density.

To further demonstrate the structural superiority of 3DC-CFs matrix for advanced electrode application, Si nanoparticles and polypyrrole-coated $NiCo_2S_4$ nanoparticles encapsulated in the 3DC-CFs structure were also tested them as anodes in LIBs (Figure S14). They showed the best cycle stability reported thus far for anodes made of Si and metal sulfide nanostructures.[50-53] These results suggest that the present 3DC-CF structure could be a versatile framework for hosting a wide range of cathode and anode materials for preparing high performance electrode (both cathode and anode) for LIB applications.

Figure 4

Conclusion

In summary, V_2O_5/3DC-CFs composite was successfully prepared as a cathode for LIBs. The special compositional and structural design of the composite enables effective

loading of V_2O_5 nanoparticles and provides good electron and ion transport capability. Effective encapsulation of the V_2O_5 nanoparticles in the 3DC can suppress SEI formation on surface of most V_2O_5 nanoparticles. On the other hand, the 3DC-CFs could be directly used of as a current collector without addition of binders and conducting materials, and the robust structure of 3DC-CFs endure the influence of volume change of active materials during cycling. As a result, the V_2O_5/3DC-CF composite delivered outstanding specific capacity, high rate performance, and extraordinary cycling stability. At a high current density of 10 C, a capacity of 183 mAh g^{-1} was obtained, which is higher than that of the current lithium transition-metal oxide cathode. In particular, the cathode demonstrated capacity retention close to 100 % at 10 C after 5000 cycles, implying the best stability of cathode materials reported thus far. The outstanding overall properties of the V_2O_5/3DC-CF composite make it a promising candidate as the cathode for high-performance LIBs.

Experimental Section

Materials synthesis. All chemicals used in this work were commercially available from Sigma-Aldrich and were used as received without further purification. The V_2O_5/3DC-CFs composites were synthesized by combining carbonization with a simple hydrothermal synthesis followed by an annealing process, which is described in Supplementary Information I in detail.

Characterization. Morphology and microstructure of samples were characterized by scanning electron microscopy (SEM, Philips XL 30FEG) and TEM (JEM-2100F equipped with an energy-dispersive X-ray spectrometer (EDS)). The X-ray diffraction (XRD) patterns were recorded using a Philips X'Pert MRD X-ray diffractometer with Cu K$_\alpha$

radiation. The *in situ* TEM observation of lithiation and dethiation processes was carried out using a scanning tunneling microscopy (STM)-TEM holder commercialized by Nanofactory Instruments AB within the JEOL 2100F TEM operated at 200 kV.

Electrochemical measurements. The V_2O_5/3DC-CFs composites were directly used as the working electrode without any ancillary materials. To measure the mass of active materials, 6 pieces of 3DC-CFs and V_2O_5/3DC-CFs composite of the same size were weighted by using an electronic balance (Sartorius BP 211D) with a resolution of 0.01 mg, and their average masses were obtained. By subtracting the average mass of 3DC-CFs, the masses of V_2O_5 (active material) synthesized in different samples were 0.52 ± 0.03, 1.18 ± 0.04, 2.48 ± 0.08 and 3.17 ± 0.13 mg cm^{-2}. The uncertainty in the average mass of 3DC-CFs thus led to an error of about ± 5% in the mass of V_2O_5. Coin-type cells (CR2032) were fabricated using lithium metal as the counter electrode, Celgard 2400 as the separator, and $LiPF_6$ (1 M) in ethylene carbonate-dimethyl carbonate (EC-DMC, 1:1 vol%) as the electrolyte. For comparison, a control sample by mixing the V_2O_5 nanoparticles, conductive agent (carbon black) and binder (sodium alginate) in a weight ratio of 50:40:10 was prepared, and another one comprising V_2O_5 nanosheet arrays/carbon fiber composite was also tested without any ancillary materials. The loading weight of the V_2O_5 nanoparticles and V_2O_5 nanosheet arrays was about 0.85 mg cm^{-2} and 1.33 mg cm^{-2}, respectively. Cyclic voltammetry (CV) measurements were conducted at 0.1 mV s^{-1} over the range of 2.0-4.0 V (vs. Li/Li$^+$) on a CHI 600D electrochemical workstation. Electrochemical impedance spectroscopy (EIS) was carried out with a ZAHNERelektrik IM 6 electrochemical system over a frequency range of 100 kHz to 0.01 Hz.

Supporting Information

Supporting Information is available from the Wiley Online Library or from the author.

[1] M. T. McDowell, S. W. Lee, W. D. Nix, Y. Cui, *Adv. Mater.* **2013**, *25*, 4966.

[2] M. J. Armstrong, C. O'Dwyer, W. J. Macklin, J. D. Holmes, *Nano Res.* **2014**, *7*, 1.

[3] J. X. Zhu, D. Yang, Z. Y. Yin, Q. Y. Yan, H. Zhang, *Small* **2014**, *10*, 3480.

[4] D. D. Vaughn II, R. E. Schaak, *Chem. Soc. Rev.* **2013**, *42*, 2861.

[5] M. V. Reddy, G. V. Subba Rao, B. V. R. Chowdari, *Chem. Rev.* **2013**, *113*, 5364.

[6] N. Liu, Z. D. Lu, J. Zhao, M. T. McDowell, H. W. Lee, W. T. Zhao, Y. A. Cui, *Nat. Nanotechnol.* **2014**, *9*, 187.

[7] M. S. Islam, C. A. J. Fisherb, *Chem. Soc. Rev.* **2014**, *43*, 185.

[8] M. Freire, N. V. Kosova, C. Jordy, D. Chateigner, O. I. Lebedev, A. Maignan, V. Pralong, *Nat. Mater.* **2016**, *15*, 173.

[9] F. Lin, D. Nordlund, Y. Y. Li, M. K. Quan, L. Cheng, T. C. Weng, Y. J. Liu, H. L. Xin, M. M. Doe, *Nature Energy* **2016**, *11*, 15004.

[10] Y. K. Sun, Z. H. Chen, H. J. Noh, D. J. Lee, H. G. Jung, Y. Ren, S. Wang, C. S. Yoon, S. T. Myung, K. Amine, *Nat. Mater.* **2012**, *11*, 942.

[11] P. Liu, S. H. Lee, C. E. Tracy, Y. Yan, J. A. Turner, *Adv. Mater.* **2002**, *14*, 27.

[12] A. Pan, H. B. Wu, L. Yu, X. W. Lou, *Angew. Chem. Int. Edit.* **2013**, *125*, 2282.

[13] M. Okubo, E. Hosono, J. Kim, M. Enomoto, N. Kojima, T. Kudo, H. S. Zhou, I. Honma, *J. Am. Chem. Soc.* **2007**, *129*, 7444.

[14] W. Tang, Y. Y. Hou, F. X. Wang, L. L. Liu, Y. P. Wu, K. Zhu, *Nano Lett.* **2013**, *13*, 2036.

[15] L. M. Guo, Y. L. Zhang, J. W. Wang, L. P. Ma, S. C. Ma, Y. T. Zhang, E. K. Wang, Y. J. Bi, D. Y. Wang, W. C. McKee, Y. Xu, J. T. Chen, Q. H. Zhang, C. W. Nan, L. Gu, P. G. Bruce, Z. Q. Peng, *Nat. Commun.* **2015**, *6*, 7898.

[16] C. Z. Wu, F. Feng, Y. Xie, *Chem. Soc. Rev.* **2013**, *42*, 5157.

[17] T. Watanabe, Y. Ikeda, T. Ono, M. Hibino, M. Hosoda, K. Sakai, T. Kudo, *Solid State Ionics* **2002**, *151*, 313.

[18] J. Y. Wang, H. J. Tang, L. J. Zhang, H. Ren, R. B. Yu, Q. Jin, J. Qi, D. Mao, M. Yang, Y. Wang, P. R. Liu, Y. Zhang, Y. R. Wen, L. Gu, G. H. Ma, Z. G. Su, Z. Y. Tang, H. J. Zhao, D. Wang, *Nature Energy* **2016**, *1*, 16050.

[19] Q. Y. An, P. F. Zhang, F. Y. Xiong, Q. L. Wei, J. Z. Sheng, Q. Q. Wang, L. Q. Mai, *Nano Res.* **2015**, *8*, 481.

[20] J. W. Lee, S. Y. Lim, H. M. Jeong, T. H. Hwang, J. K. Kang, J. W. Choi, *Energy Environ. Sci.* **2012**, *5*, 9889.

[21] H. Liu, W. Yang, *Energy Environ. Sci.* **2011**, *4*, 4000.

[22] M. M. Rahman, A. Z. Sadek, I. Sultana, M. Srikanth, X. J. J. Dai, M. R. Field, D. G. McCulloch, S. B. Ponraj, Y. Chen, *Nano Research* 2015, 8, 3591.

[23] S. Mateti, M. M. Rahman, L. H. Li, Q. R. Caia, Y. Chen, *RSC Adv.* 2016, 6, 35287.

[24] M. Sathiya, A. Prakash, K. Ramesha, J. M. Tarascon, A. K. Shukla, *J. Am. Chem. Soc.* **2011**, *133*, 16291.

[25] X. Y. Chen, H. L. Zhu, Y. C. Chen, Y. Y. Shang, A. Y. Cao, L. B. Hu, G. W. Rubloff, *ACS Nano* **2012**, *6*, 7948.

[26] X. F. Zhang, K. X. Wang, X. Wei, J. S. Chen, *Chem. Mater.* **2011**, *23*, 5290.

[27] Y. L. Cheah, R. von Hagen, V. Aravindan, R. Fiz, S. Mathur, S. Madhavi, *Nano Energy* **2013**, *2*, 57.

[28] Q. Liu, Z. F. Li, Y. D. Liu, H. Y. Zhang, Y. Ren, C. J. Sun, W. Q. Lu, Y. Zhou, L. Stanciu, E. A. Stach, J. Xie, *Nat. Commun.* **2015**, *6*, 6127.

[29] D. McNulty, D. Noel Buckley, C. O'Dwyer, *J. Power Sources* **2014**, *267*, 831.

[30] D. L. Chao, X. H. Xia, J. L. Liu, Z. X. Fan, C. F. Ng, J. Y. Lin, H. Zhang, Z. X. Shen, H. J. Fan, *Adv. Mater.* **2014**, *26*, 5794.

[31] X. Y. Yu, Z. Y. Lu, G. X. Zhang, X. D. Lei, J. F. Liu, L. Wang, X. M. Sun, *RSC Adv*. **2013**, *3*, 19937.

[32] J. Yan, A. Sumboja, E. Khoo, P. S. Lee, *Adv. Mater.* **2011**, *23*, 746.

[33] H. Wu, G. Chan, J. W. Choi, I. Ryu, Y. Yao, M. T. McDowell, S. W. Lee, A. Jackson, Y. Yang, L. B. Hu, Y. Cui, *Nat. Nanotechnol.* **2012**, *7*, 310.

[34] Q. B. Zhang, H. X. Chen, J. X. Wang, D. G. Xu, X. H. Li, Y. Yang, K. L. Zhang, *ChemSusChem* **2014**, *7*, 2325.

[35] L. Q. Mai, F. Dong, X. Xu, Y. Z. Luo, Q. Y. An, Y. L. Zhao, J. Pan, J. N. Yang, *Nano Lett.* **2013**, *13*, 740.

[36] Y. W. Li, J. H. Yao, E. Uchaker, J. W. Yang, Y. X. Huang, M. Zhang, G. Z. Cao, *Adv. Energy Mater.* **2013**, *3*, 1171.

[37] J. K. Shon, H. S. Lee, G. O. Park, J. Yoon, E. Park, G. S. Park, S. S. Kong, M. S. Jin, J. M. Choi, H. Chang, S. Doo, J. M. Kim, W. S. Yoon, C. Pak, H. Kim, G. D. Stucky, *Nat. Commun.* **2016**, *7*, 11049.

[38] Q. B. Zhang, H. X. Chen, J. X. Wang, D. G. Xu, X. H. Li, Y. Yang, K. L. Zhang, *ChemSusChem* **2014**, *7*, 2325.

[39] J. Yang, H. Wang, P. F. Hu, J. J. Qi, L. Guo, L. H. Wang, A *Small* **2015**, *11*, 3744.

[40] X. F. Wang, B. Liu, X. J. Hou, Q. F. Wang, W. W. Li, D. Chen, G. Z. Shen, *Nano Res.* **2014,** *7*, 1073.

[41] Q. L. Wei, Q. Y. An, D. D. Chen, L. Q. Mai, S. Y. Chen, Y. L. Zhao, K. M. Hercule, L. Xu, A. M. Khan, Q. J. Zhang, *Nano Lett.* **2014**, *14*, 1042.

[42] L. Q. Mai, Q. L. Wei, Q. Y. An, X. C. Tian, Y. L. Zhao, X. Xu, L. Xu, L. Chang, Q. J. Zhang, *Adv. Mater.* **2013**, *25*, 2969.

[43] Z. Y. Wang, Y. F. Dong, H. J. Li, Z. B. Zhao, H. B. Wu, C. Hao, S. H. Liu, J. S. Qiu, X. W. Lou, *Nat. Commun.* **2014**, *5*, 5002.

[44] J. Y. Huang, L. Zhong, C. M. Wang, J. P. Sullivan, W. Xu, L. Q. Zhang, S. X. Mao, N. S. Hudak, X. H. Liu, A. Subramanian, H. Y. Fan, L. Qi, A. Kushima, J. Li, *Science* **2010**, *330*, 1515.

[45] E. Strelcov, J. Cothren, D. Leonard, A. Y. Borisevichc, A. Kolmakovd, *Nanoscale* **2015**, *7*, 3022.

[46] R. J. Zou, Z. Y. Zhang, M. F. Yuen, M. L. Sun, J. Q. Hu, C. S. Lee, W. J. Zhang, *NPG Asia Materials* **2015**, *7*, e195.

[47] D. L. Chao, C. R. Zhu, X. H. Xia, J. L. Liu, X. Zhang, J. Wang, P. Liang, J. Y. Lin, H. Zhang, Z. X. Shen, H. J. Fan, *Nano Lett.* **2015**, *15*, 565.

[48] J. Pan, J. Q. Deng, Q. R. Yao, Y. J. Zou, Z. M. Wang, H. Y. Zhou, L. X. Sun, G. H. Rao, *J. Power Sources* **2015**, *288*, 353.

[49] Y. X. Tang, Y. Y. Zhang, J. Y. Deng, J. Q. Wei, H. L. Tam, B. K. Chandran, Z. L. Dong, Z. Chen, X. D. Chen, *Adv. Mater.* **2014**, *26*, 6111.

[50] H. Wu, Y. Cui, *Nano Today* **2012**, *7*, 414.

[51] J. R. Szczech, S. Jin, *Energy Environ. Sci*. **2011**, *4*, 56.

[52] X. D. Xu, W. Liu, Y. Kim, J. Cho, *Nano Today* **2014**, *9*, 604.

[53] X. H. Rui, H. T. Tan, Q. Y. Yan, *Nanoscale* **2014**, *6*, 9889.
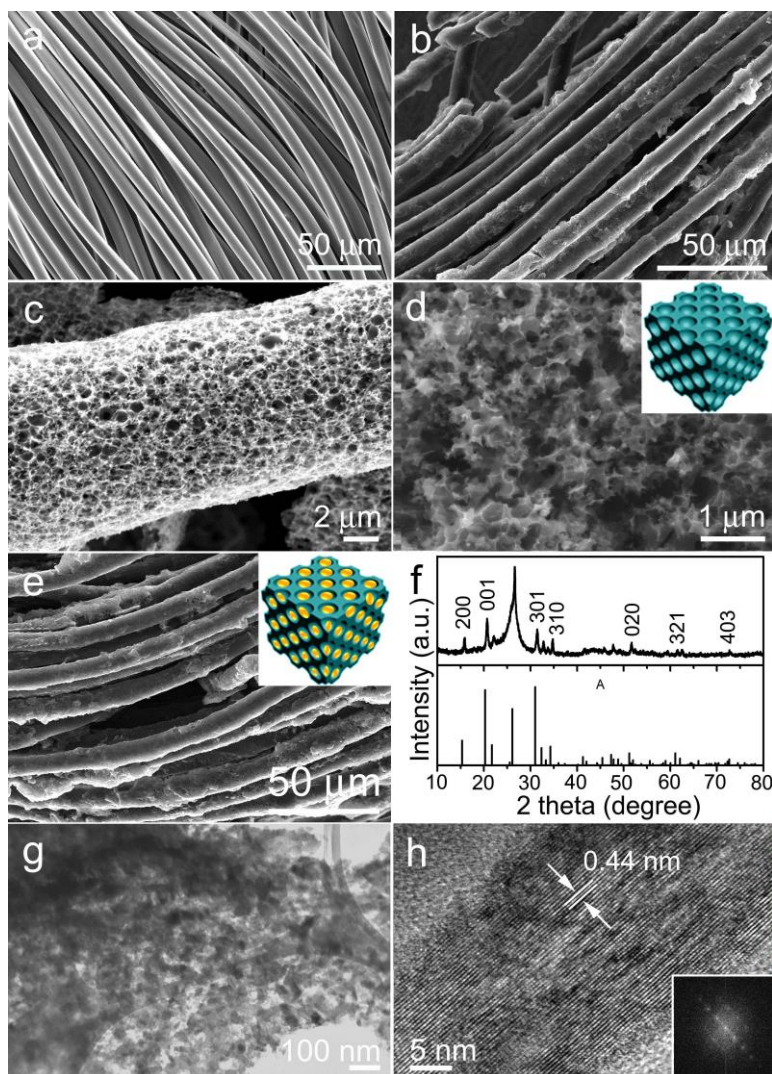
Figure 1. (a) SEM image of CFs coated with polymer carbon-precursor layer. (b), (c), and (d) SEM images of the 3D networked carbon matrix film-coated CFs at different magnifications, the inset in (d) shows the schematic drawing of the 3D networked porous carbon matrix. (e) SEM image of the V_2O_5/3DC-CFs composite, the inset shows the schematic drawing of the V_2O_5/3DC composite structure. (f) XRD patterns of the V_2O_5/3DC-CFs composite (upper panel) and JCPDS card (V_2O_5, No. 41-1426) (lower panel). (g) TEM image of the V_2O_5/3DC composite. (h) HRTEM image of a V_2O_5 nanoparticle, the inset shows the corresponding FFT pattern.
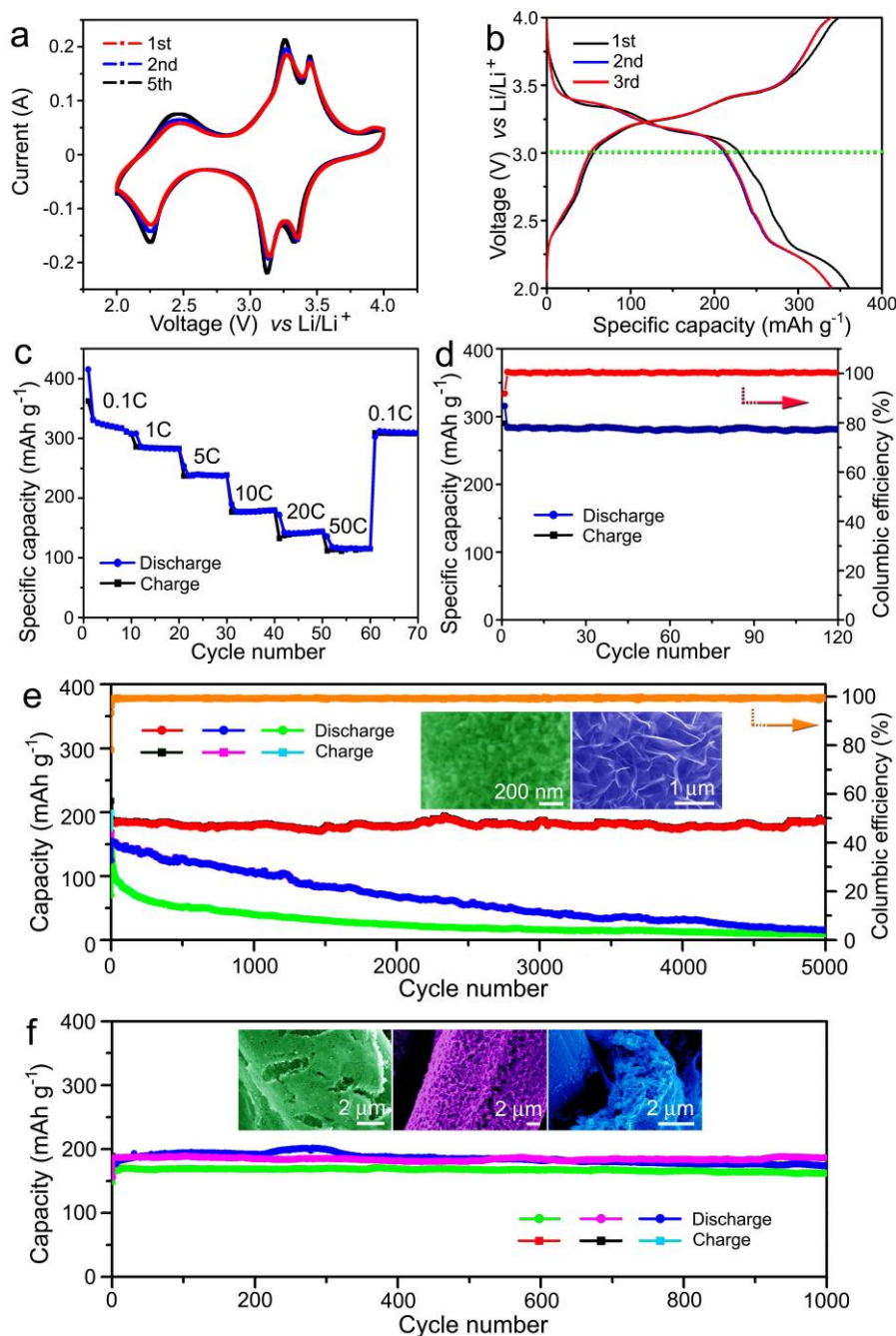
Figure 2. (a) CV curves of V_2O_5/3DC-CFs composite at a scan rate of 0.1mV s^{-1} between 4.0 and 2.0 V. (b) Charge-discharge curves of V_2O_5/3DC-CFs composite at a constant current density of 0.1C between 4.0 and 2.0 V. (c) Rate performance of 3D networked V_2O_5/3DC-CFs electrode at various current densities. (d) Cycling performance and corresponding Coulombic efficiency of V_2O_5/3DC-CFs composite measured at 1C. (e) Cycling performance of V_2O_5/3DC-CFs composite, V_2O_5 nanoparticles and V_2O_5 nanosheet arrays electrodes measured at 10 C. The insets are the SEM morphologies of

V_2O_5 nanoparticle (left) and V_2O_5 nanosheet array (right) electrodes. (f) Cycling performance of V_2O_5/3DC-CFs composite electrode with different loading of V_2O_5 nanoparticles measured at 10 C. The insets are the SEM morphologies of the composite electrodes with mass loadings of 0.52 mg cm^{-2} (left), 2.48 mg cm^{-2} (middle) and 3.17 mg cm^{-2} (right).
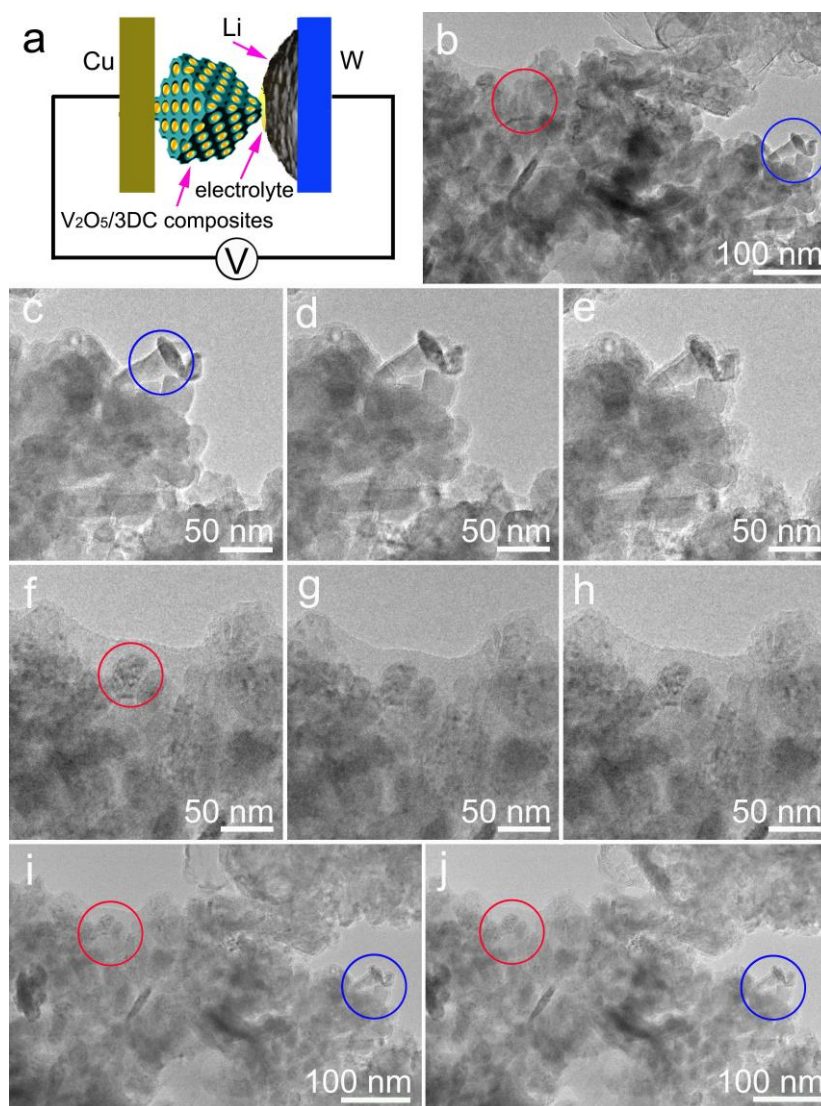
Figure 3. (a) Schematic showing the configuration of *in situ* TEM observation for Li$^+$ insertion and extraction processes. (b) TEM images of the pristine V_2O_5/3DC composite before lithium insertion. The red and blue circles indicate the V_2O_5

nanoparticles inside and at the edge of the 3DC matrix, respectively. (c-e) Morphology evolution of the V₂O₅ nanoparticles at the edge of the matrix during the Li⁺ insertion processes at 1 min, 5 min and 20 min, respectively. (f-h) Morphology evolution of the V₂O₅ nanoparticles inside the 3DC matrix during the Li⁺ insertion processes at 1 min, 5 min and 20 min, respectively. (i) TEM image of the V₂O₅/3DC composite after Li⁺ extraction processes in the first cycle. (j) TEM image of the V₂O₅/3DC composite after Li⁺ extraction processes in the 10th cycle.
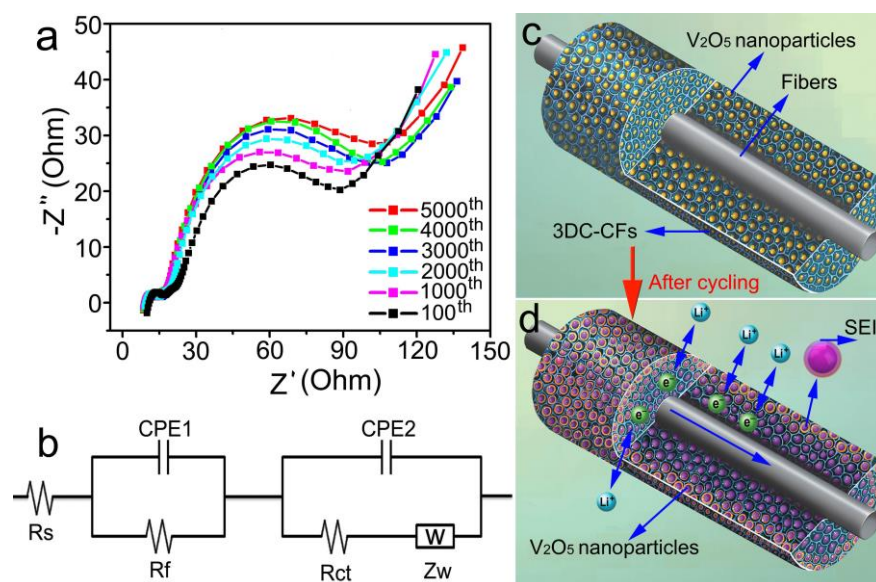
Figure 4. (a) Nyquist plots of the V₂O₅/3DC-CFs composite electrode measured with an amplitude of 5 mV over a frequency range from 100 kHz to 0.01 Hz; (b) the equivalent circuit model of V₂O₅/3DC-CFs composite electrode. R_s is the electrolyte resistance; CPE1 and R_f are the capacitance and resistance of the passivation film formed on the electrode surface, respectively; CPE2 and R_{ct} are the double-layer capacitance and charge transfer resistance, respectively; and Zw is the Warburg impedance related to the diffusion of lithium ions into the bulk of the electrode. (c) Schematic of V₂O₅/3DC-CFs composite before electrochemical cycling. (d) Schematic diagrams showing the

formation of SEI layer, and the transport of electrons and Li ions in V_2O_5/3DC-CFs composite.

Full Paper

We report a new cathode material for lithium ion batteries consist of V_2O_5 nanoparticles encapsulated in 3D network porous carbon matrix layer coated on carbon fibers. The cathode delivers a higher capacity as compared to the current lithium transition-metal oxide cathode, and much superior cyclic stability with an almost 100% capacity retention at a high current density of 10 C after 5000 cycles.

Rujia Zou, Qian Liu, Guanjie He, Muk Fung Yuen, Kaibing Xu, Junqing Hu*, Ivan P. Parkin, Chun-Sing Lee* and Wenjun Zhang*

Nanoparticles Encapsulated in Porous Carbon Matrix Coated on Carbon Fibers: An Ultrastable Cathode for Li-Ion Batteries

ToC figure
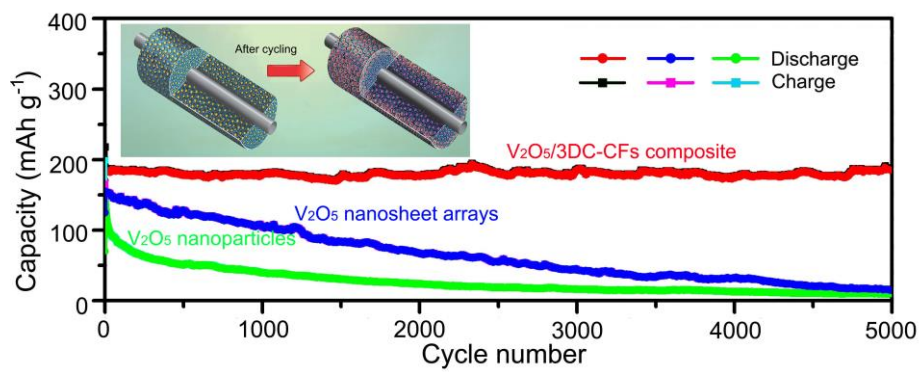
Supporting Information

Nanoparticles Encapsulated in Porous Carbon Matrix Coated on Carbon Fibers: An Ultrastable Cathode for Li-Ion Batteries

Rujia Zou, Qian Liu, Guanjie He, Muk Fung Yuen, Kaibing Xu, Junqing Hu,* Ivan P. Parkin, Chun-Sing Lee,* and Wenjun Zhang*

Dr. R. Zou, Dr. Y. Liu, Dr. K. Xu, Prof. J. Hu

State Key Laboratory for Modification of Chemical Fibers and Polymer Materials, College of Materials Science and Engineering, Donghua University, Shanghai 201620, China

E-mail: hu.junqing@dhu.edu.cn

Dr. M. Yuen, Prof. C. Lee, Prof. W. Zhang

Center of Super-Diamond and Advanced Films (COSDAF), Department of Physics and Materials Science, City University of Hong Kong, Hong Kong

E-mail: apcslee@cityu.edu.hk; and apwjzh@cityu.edu.hk

Dr. G. He, Prof. I. Parkin

Materials Chemistry Centre, Department of Chemistry, University College London, 20 Gordon Street, London WC1H 0AJ, UK

Figure S1. Raman spectrum of 3DC layer coated on carbon cloth.
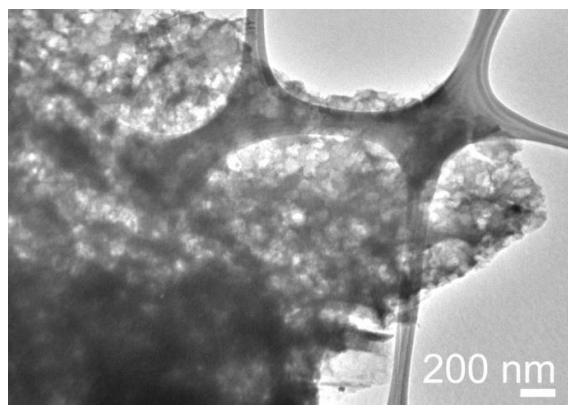
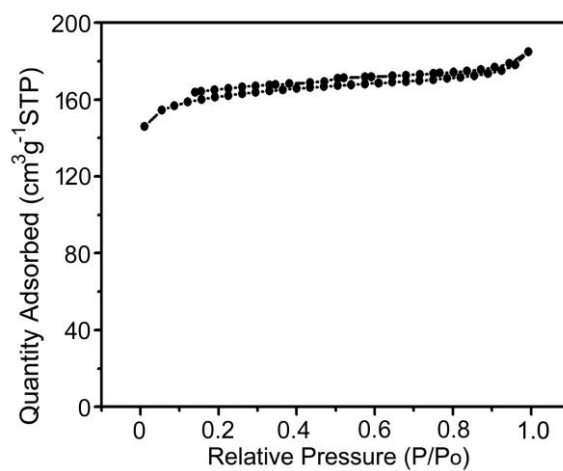**Figure S2.** TEM image of the 3D networked porous carbon layer.

Figure 3. N$_2$ adsorption/desorption isotherms of the networked porous carbon matrix.

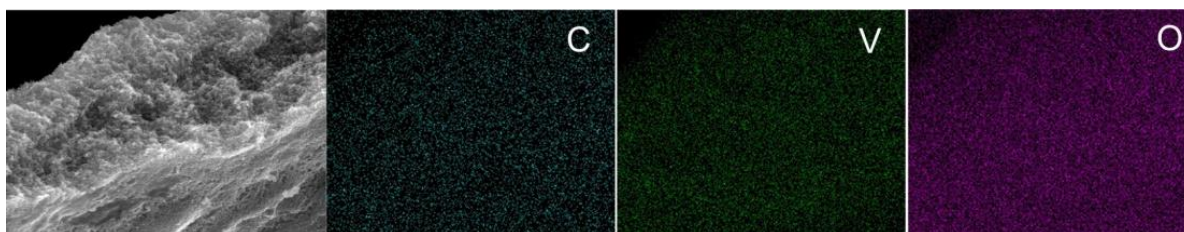**Figure S4.** The V$_2$O$_5$/3DC-CF composite shows excellent flexibility.

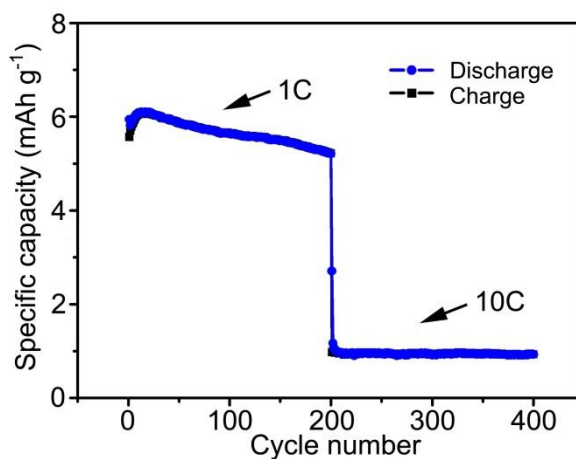**Figure S5.** SEM and Elemental mapping images of the V$_2$O$_5$/3DC-CFs composite.

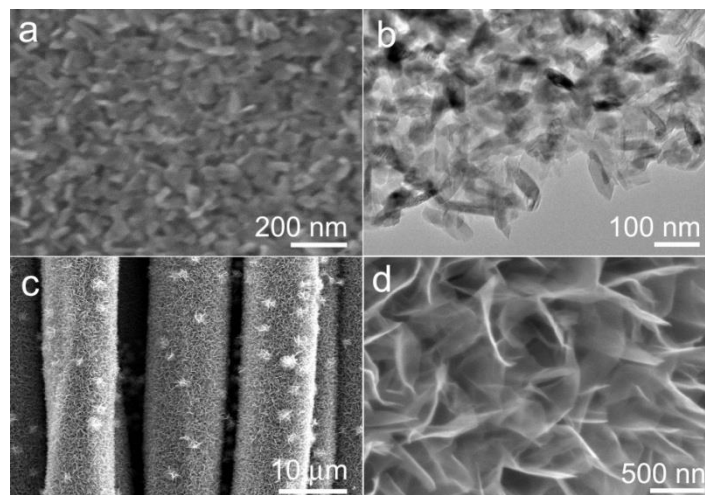**Figure S6.** Cycling performance of 3DC coated carbon cloth (3DC-CC) electrode at 1C and 10C.

Figure S7. TEM and SEM characterizations of V_2O_5 nanoparticles and V_2O_5 nanosheet arrays on carbon fibers. (a) SEM and (b) TEM images of V_2O_5 nanoparticles; (c) and (d) SEM images of V_2O_5 nanosheet arrays on carbon fibers at the different magnifications.
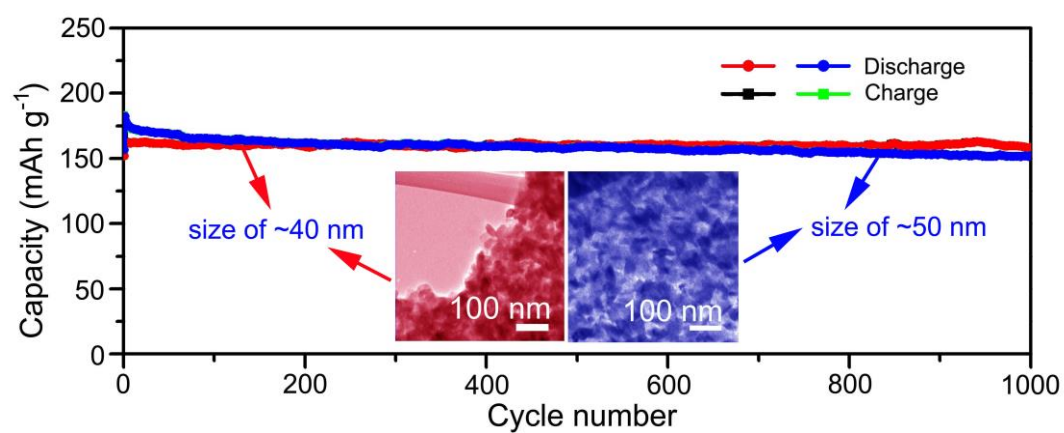

Figure S8. The cycling stability of V_2O_5 nanoparticles of ~40 (red, insert left) and ~50 nm (blue, insert right) in size encapsulated in 3D network porous carbon as cathode for application in LIBs.
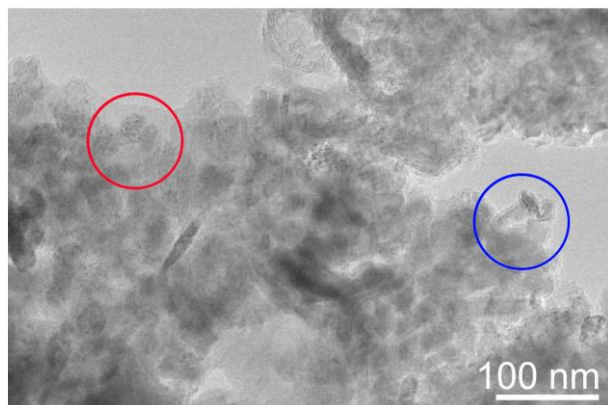
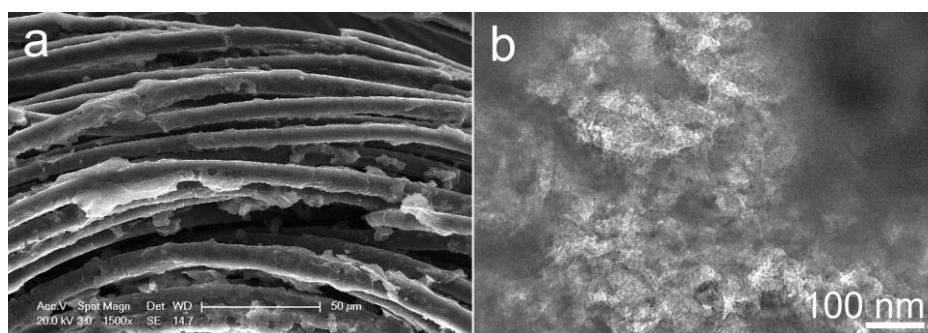**Figure S9.** TEM images of the V$_2$O$_5$/3DC composite with lithium insertion at 20 min in the first cycle.

Figure S10. (a) SEM and (b) TEM images of V$_2$O$_5$/3DC-CF composite after 5000 cycles.
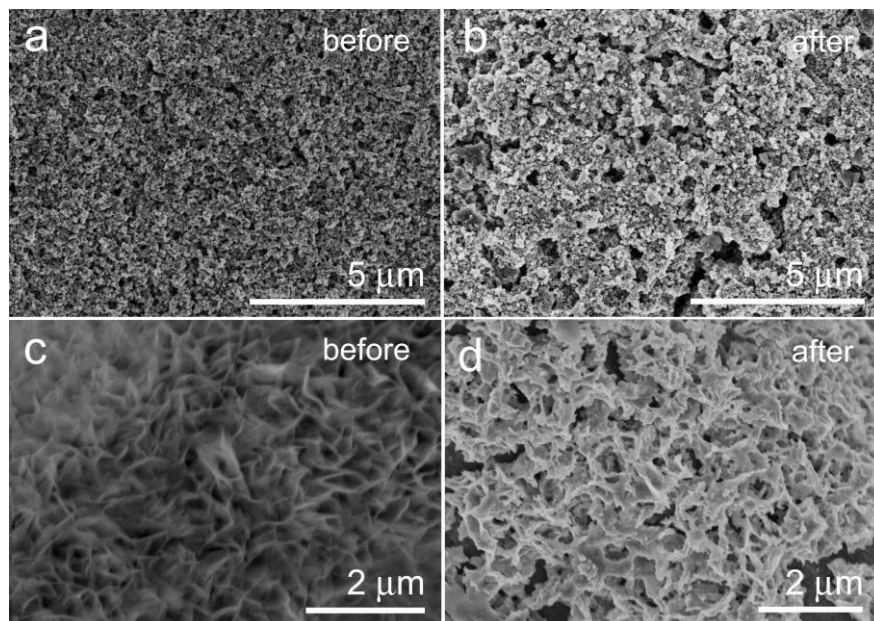
Figure S11. SEM images of V_2O_5 nanoparticle (a) before and (b) after test for 5000 cycles, and   SEM images of V_2O_5 nanosheet arrays (c) before and (b) after test for 5000 cycles. For the V_2O_5 nanosheet arrays electrode, the nanosheets are anchored to the current collector (carbon fibers) without binder and conductive carbon.
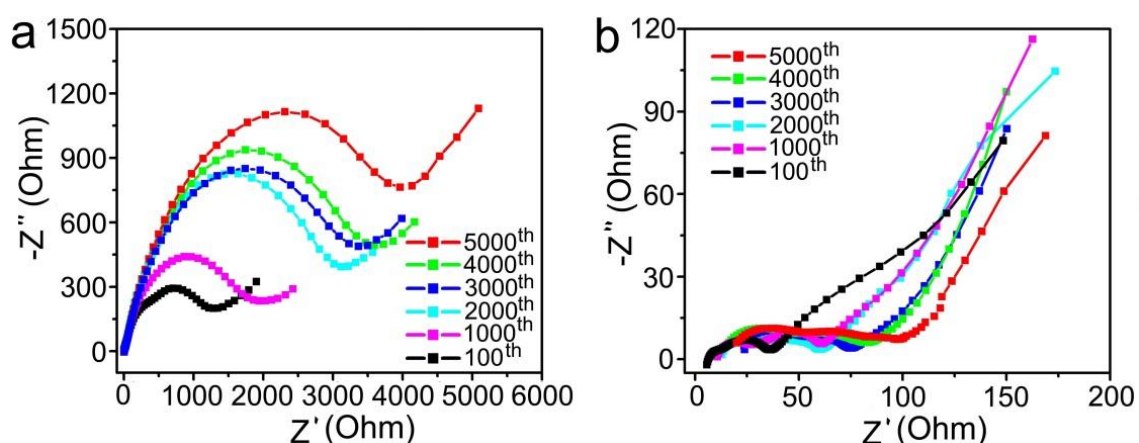

Figure S12. Nyquist plots of (a) V_2O_5 nanoparticle and (b) V_2O_5 nanosheet array electrodes measured with amplitude of 5 mV over a frequency range from 100 kHz to 0.01 Hz.

Table S1. R_{ct} and R_f for V_2O_5/3DC-CFs electrode, V_2O_5 nanoparticles electrode and V_2O_5 nanoparticles electrode by modified equivalent circuit model.

| Cycle | \multicolumn{6}{c}{V_2O_5/3DC-CFs electrode} | | | | | | \multicolumn{6}{c}{V_2O_5 nanoparticles electrode} | | | | | | \multicolumn{6}{c}{V_2O_5 nanoparticles electrode} |

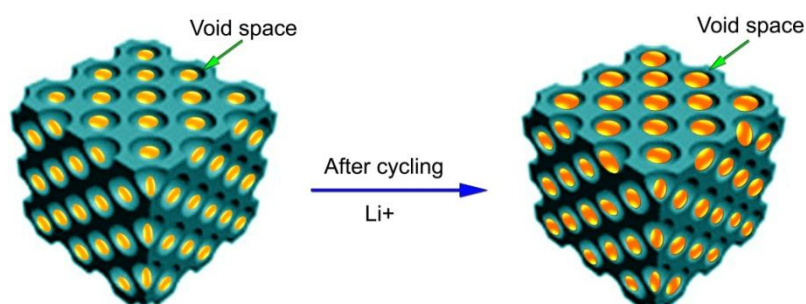| Cycle	100	1000	2000	3000	4000	5000	100	1000	2000	3000	4000	5000	100	1000	2000	3000	4000	5000
R_{ct} (Ω)	171	98	103	95	97	88	1400	1900	3300	3800	3500	4500	71	78	89	109	122	138
R_f (Ω)	9.2	10.5	8.9	8.8	9.4	10.8	19.1	24.3	25.1	26.4	23.5	30.5	6.4	9.9	12.1	18.2	20.6	22.5

Figure S13. 3D view inside V_2O_5/3DC-CF composite before and after electrochemical cycling (in the lithiated state).
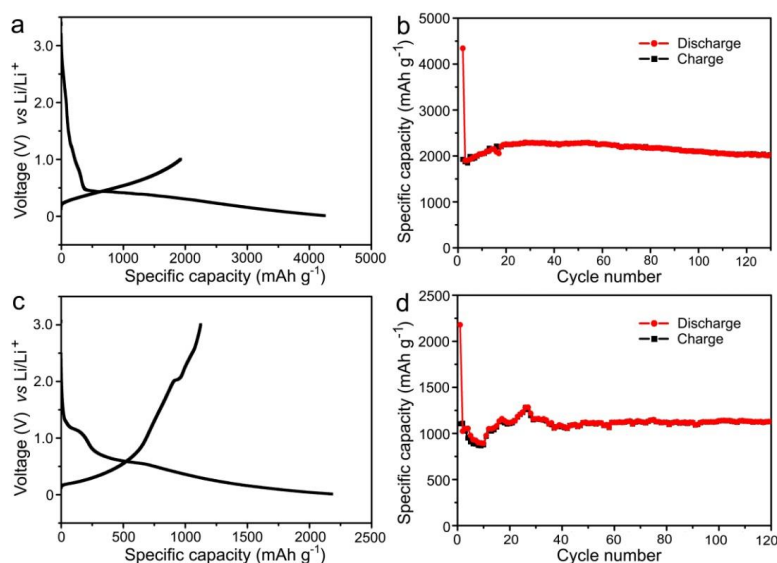
Figure S14. Si nanoparticles and polypyrrole-coated $NiCo_2S_4$ nanoparticles encapsulated in the 3DC-CFs structure were tested them as anodes in LIBs. (a) CV curves of Si/3DC-CF composite at a scan rate of 0.1 mVs^{-1} between 0.01 and 1.0 V. (b) Cycling performance of Si/3DC-CF composite measured at 0.5C. (c) CV curves of $NiCo_2S_4$-PPy/3DC-CF composite at a scan rate of 0.1 mVs^{-1} between 0.01 and 3.0 V. (d) Cycling performance of $NiCo_2S_4$-PPy/3DC-CF composite measured at 1000 mA g^{-1}. To further demonstrate the structural superiority of 3DC-CFs matrix for advanced electrode application, Si nanoparticles and PPy-coated $NiCo_2S_4$ nanoparticles encapsulated in the 3DC-CFs structure were synthesized using the simple hydrothermal methods, and apply them as anodes in LIBs. Excitedly, the electrodes of Si/3DC-CFs and PPy-$NiCo_2S_4$/3DC-CFs composites also show remarkable battery performance. For the electrode of Si/3DC-CFs composites (Figures S13a and b), a high capacity of 1899 mAh g^{-1} was obtained at fouth cycle (the activation of materials by pre-cycling three cycles), and it could be retained at 2028 mAh g^{-1} after 130 cycles at a current density of 0.5C, indicating an superior cycle stability as compare with reported for electrodes made of Si nanostructures.[1,2] For the electrode of PPy-$NiCo_2S_4$/3DC-CFs composite (Figures S13c and d), a capacity of 1054 mAh g^{-1} was obtained at fouth cycle, and it could be retained

at 1129 mAh g^{-1} after 120 cycles at a current density of 1000 mA g^{-1}, the best cycle stability reported thus far for electrodes made of metal sulfide nanostructures or their composites.[3,4] Those results reveal that the 3DC-CFs structure have potential applications as high-performance LIBs of both cathode and anode electrodes

References

1 H. Wu, Y. Cui, *Nano Today* **2012**, *7*, 414.

2 J. R. Szczech, S. Jin, *Energy Environ. Sci*. **2011**, *4*, 56.

3 X. D. Xu, W. Liu, Y. Kim, J. Cho, *Nano Today* **2014**, *9*, 604.

4 X. H. Rui, H. T. Tan, Q. Y. Yan, *Nanoscale* **2014**, *6*, 9889.

Synthesis of materials

Preparation of the V_2O_5/3DC-CFs composite involves two processes as described below:

i) Preparation of 3D networked porous carbon matrix: Amylum (5g) and KOH (5g) were mixed in 40 mL deionized water under vigorous agitation in a beaker (50 mL), and then transferred into an electric oven and kept at 60 ^{o}C for 24 h to form a sol-gel solution. A piece of carbon cloth was first soaked in the sol-gel solution for 1 hours at 80 ^{o}C, and then taken out and dried at 80 ^{o}C for 24 h. The sample was then carbonized by heating in a tubular furnace under a nitrogen atmosphere at 600 ^{o}C for 2 h with a heating rate of 2 ^{o}C min^{-1}, and successively washed with dilute HCl and distilled water, and cleaned by ultrasonication to remove the loosely attached carbon materials. Finally, the sample was dried at 80 °C for 24 h in a vacuum oven to obtain a piece of 3D networked porous carbon matrix coated flexible carbon fibers (3DC-CFs). The areal loading of the 3D networked porous carbon matrix was estimated to be 0.42 ± 0.02 mg/cm^2.

ii) Synthesis of V_2O_5 nanoparticles encapsulated in 3D networked porous carbon matrix: 0.01 mL of vanadium triisopropoxide oxide was added into 40 mL of isopropanol alcohol (IPA) under vigorous stirring for 30 min. The mixture solution and a piece of the prepared 3DC-CFs were transferred into an autoclave which is loaded into an electric oven and held for 13 h at 180 ^{o}C. The samples were washed with deionized water and ethanol successively to remove the residual ionic species and then dried in vacuum for 24 h. The dried sample was further annealed in air at 320 ^{o}C for 2 h to obtain V_2O_5 nanoparticles encapsulated in 3D networked porous carbon matrix.

For comparison, a control sample was also prepared by synthesizing V_2O_5 directly on a

piece of the as-received carbon fibers (i.e without the 3D porous carbon surface layer).